Bull. Mater. Sci., Vol. 34, No. 2, April 2011, pp. 217–226. © Indian Academy of Sciences.

Multiple strengthening mechanisms in nanoparticle-reinforced copper matrix composites

D BOZIC, J STASIC, B DIMCIC, M VILOTIJEVIC and V RAJKOVIC*
Institute of Nuclear Sciences "Vinca", University of Belgrade, 11001 Belgrade, Serbia

MS received 6 July 2010; revised 8 December 2010

Abstract. The multiple hardening mechanisms of a copper matrix have been presented and discussed. The prealloyed ball milled Cu–3 wt.%Al and the atomized Cu–0·6 wt.%Ti–2·5 wt.%TiB_2 powders have been used as starting materials. Dispersoid particles Al_2O_3 and TiB_2 were formed *in situ*. The powders have been hot consolidated. Optical microscopy, SEM, TEM, and X-ray diffraction analysis were performed for microstructural characterization. Increase in microhardness of Cu–3 wt.%Al compacts is a consequence of the crystallite size refinement and the presence of Al_2O_3 particles. High hardening of Cu–0·6 wt.%Ti–2·5 wt.%TiB_2 is a consequence of the presence of modular structure, $Cu_4Ti_{(m)}$, and TiB_2 particles.

Keywords. Metal–matrix composites (MMCs); nanoparticles; hardness testing; microstructural characterization.

1. Introduction

Copper matrix composites have a wide range of applications because of the combination of high mechanical strength and electrical/thermal conductivity. To improve the interfacial compatibility and avoid serious interfacial reaction, various new processing techniques are being used to fabricate ceramic particle-reinforced metal matrix composites (MMCs) (Ma *et al* 1999, 2000; Tjong *et al* 1999; Lee *et al* 2000; Tjong and Lau 2000). The basic principle of this technique is that the fine and thermodynamically stable ceramic phases are formed *in situ* by exothermal reaction between elements or between element and compound within a metal matrix. Reaction processes between structural components in obtaining particle reinforcement occur in solid or liquid state (Ralph *et al* 1997). The *in situ* composites exhibit improved mechanical strength, hardness as well as enhanced wear resistance (Kuruvilla *et al* 1990).

In situ formation of fine Al_2O_3 particles in copper matrix, in solid state, can be conducted in several ways: by mechanical alloying, where Cu–Al_2O_3 composite is obtained by milling and cold welding of ceramic particles in copper matrix in atritor (Naser *et al* 1997), mechanical alloying of Cu and $Al(OH)_3$ powders and subsequent sintering (Mehta *et al* 1990), milling of copper and aluminium powders and internal oxidation of aluminium powders (Nadkarni and Synk 1984), coprecipitation of the nitrates of copper and aluminium with ammonia, conversion of the product to oxides, reduction by hydrogen (Mehta *et al* 1990) and treating of prealloyed Cu–Al powder in high-energy ball mill in air (Rajkovic *et al* 2006). In all of these cases, the reinforcing Al_2O_3 particles size does not exceed 100 nm.

Apart from Al_2O_3 particles, TiB_2 particles are now-a-days increasingly used for copper matrix strengthening. Titanium diboride is well known for its high stiffness, hardness and high mechanical strength. Furthermore, in contrast to most ceramics, it is electrical and thermal conductive (Tu *et al* 2002). This suggests that TiB_2 is a potential reinforcing material for copper and its alloys in cases where high electrical conductivity is important. *In situ* formation of these particles in copper matrix, or copper alloys, is most frequently conducted in liquid state, by spray forming process (Lawley and Apelian 1994), reaction of B_2O_3, carbon and titanium in Cu–Ti cast (Tu *et al* 2002), or gas atomization of Cu–Ti and Cu–B cast (Bozic and Mitkov 1992). In this case, the TiB_2 particles formed are also in nanometres.

Investigations conducted in this work were related to two composite materials: one already commercial, Cu–Al_2O_3, and the other, still potential, Cu–Ti–TiB_2.

The aim of the present work includes the strengthening of a copper and copper alloy matrix by using PM techniques, appropriate choice of alloying elements and different ways for dispersoids formation as well as analysis of their single or combined effects on the strength of obtained material at room and elevated temperatures.

2. Experimental

The inert gas atomized pre-alloyed copper powder containing 3 wt.% aluminium (Cu–3 wt.% Al) and Cu–4 wt.%Ti and Cu–1·2 wt.%B alloys served as starting materials, respectively.

*Author for correspondence (visnja@vinca.rs)

The pre-alloyed copper powder, i.e. Cu–3 wt.%Al was milled up to 20 h in the planetary ball mill in air to obtain a fine grain structure and formation of alumina dispersoids by internal oxidation. The milling process was performed without introducing the additives. The weight ratio of powders to steel balls was 1:35. After milling, all powders were treated in hydrogen at 400°C for 1 h in order to eliminate copper oxides.

A mixture of electrolytic copper and titanium chips, as well as a mixture of electrolytic copper and amorphous boron, were uniaxially pressed. The green samples with determined constituent weight percentages (Cu–4 wt.%Ti and Cu–1·2 wt.%B) were separately vacuum induction melted at 1100°C, for 10 min. The heating and cooling rates during melting were 100 and 200 K min^{-1}, respectively, and casting in a copper mould was performed in an argon atmosphere. The master alloys were heated at a rate of 200 K min^{-1}. Atomization started at 1400°C and the homogenization time was 5 min. The argon pressure used was 3 MPa and the cooling rate of droplets was in the range from 10^3 to 10^6 Ks^{-1} (Bozic and Mitkov 1991).

Characterization of atomized powders included chemical analysis by means of atomic emission spectrometry, optical microscopy (OM), X-ray diffraction (XRD) analysis, sieving and microhardness measurements. A Buehler MicroMet Vickers Microindentation Hardness Tester, Model MicroMet 5101 was utilized for obtaining the powders Vickers microhardness values, applying a 15 g load.

Cu–3 wt.%Al compacts were obtained by hot pressing in an argon atmosphere at 800°C for 3 h under the pressure of 35 MPa. Compacts from 5 and 20 h milled powders were treated in argon at 800°C for 5 h with the idea to examine their thermal and electrical stability.

The atomized Cu-Ti-B powders were consolidated by hot isostatic pressing (HIP). The HIP-ing test tube was made of thin-sided copper tube, 10 mm in diameter and 200 mm in length. Tube walls were 0·8 mm thick. HIP-ing was performed at 750°C for 10 min in the argon protective atmosphere using the 'NF' press with 200 MPa maximal applied pressure, followed by the argon quenching to room temperature. Small specimens cut from compacts were solution-treated under vacuum at 900°C for 1 h, and water-quenched immediately. These specimens were aged from 300 to 600°C in steps of 50°C for different times.

The Cu–3 wt.%Al powders and compacts were characterized by X-ray diffraction analysis, optical and scanning electron microscopy (SEM). The lattice parameter was determined using the least square root method. The average lattice distortion, i.e. relative deviation of the lattice parameters from their mean value ($\Delta d/d$) and the crystallite size (D) of Cu–3 wt.%Al powder and compact was determined from the broadening (β) of the first four diffraction lines (111, 200, 220 and 311) using the approach developed by Williams and Hall (1953). The strengthening of the copper matrix was estimated by microhardness measurement (applied load was 50 g).

The optical microscope and transmission electron microscope (TEM) were used for the microstructure characterization of Cu–Ti–TiB_2 compacts. Cylindrical discs with thickness less than 100 μm were thinned by a double jet method with the same solution used for etching. The compacts density of examined materials was determined using the standard Archimedes method in xylene. The Vickers hardness tester (Buehler SemiMacro Vickers Indentation Hardness Tester, Model 1114) was utilized to determine hardness of compacts, applying the 10 kg load.

3. Results

3.1 *Cu–3 wt.%Al alloy*

The relationship between Cu–3 wt.%Al lattice parameter and milling time is shown in figure 1. The rapid decrease in lattice parameter occurs at the very beginning of the milling process, then the change in lattice parameter decreases slowly with prolonged milling. The decrease in lattice parameter is due to the oxidation of dissolved aluminium by oxigene from air, which forms alumina dispersoids. Cu–Al phase diagram is shown in figure 2 (www.semitracks.com/index.php/en/reference-material/material-properties). The difference in lattice parameters of prealloyed Cu–3 wt.%Al powders before ($a_{Cu-3\,wt.\%Al}$ = 0·36385 nm) and after 20 h of milling ($a_{Cu-3\,wt.\%Al}$ = 0·36270 nm) is 0·32%. This difference, similar to the difference (0·30%) in theoretical lattice parameters of the prealloyed powder ($a_{Cu-3\,wt.\%Al}$ = 0·36260 nm) and the copper powder (a_{Cu} = 0·36152 nm), indicates that after 20 h of milling almost all aluminium was precipitated from the copper matrix. Considering that the complete amount of aluminium was oxidized, it was calculated that 5·6 wt.% of alumina was generated

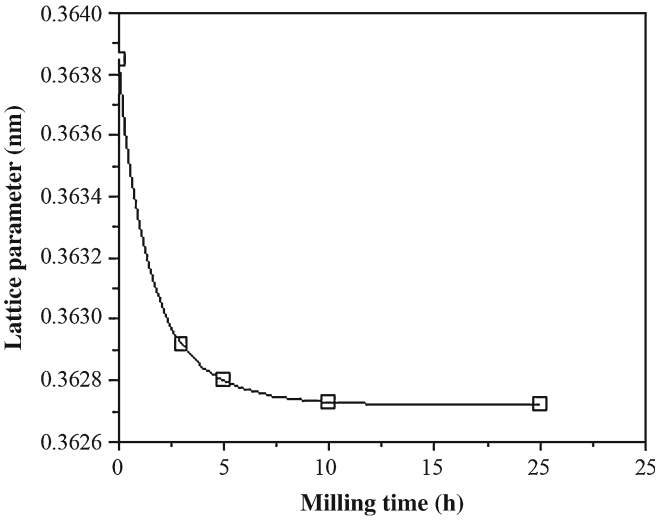

Figure 1. Lattice parameter vs milling time for Cu–3 wt.%Al powders.

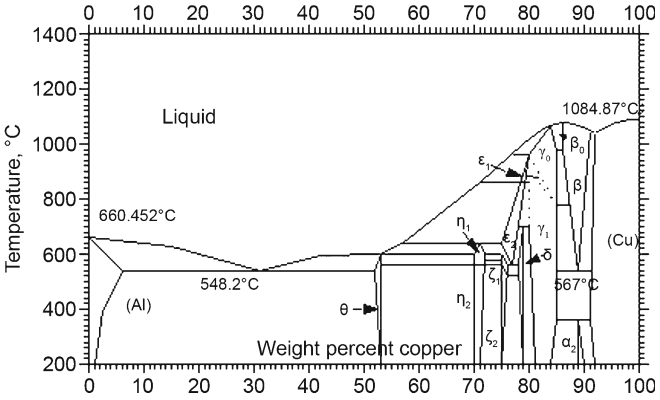

Figure 2. Cu–Al phase diagram.

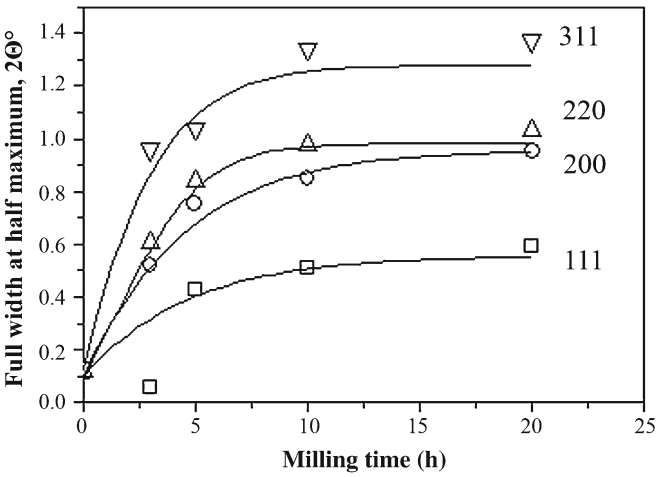

Figure 3. Full width at half maximum (FWHM) vs milling time for Cu–3 wt.%Al powders.

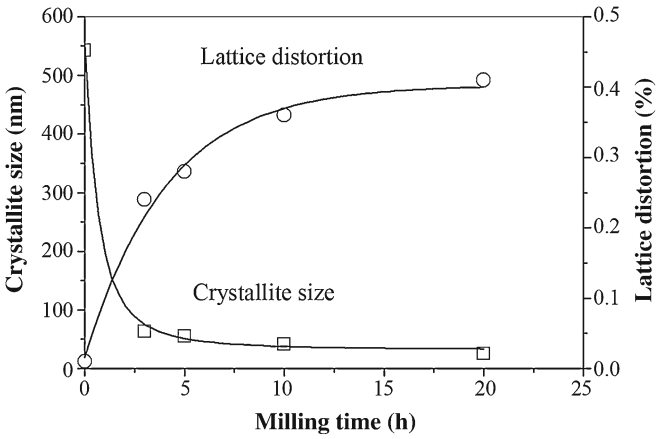

Figure 4. Effect of milling time on crystallite size and lattice distortion of Cu–3 wt.%Al.

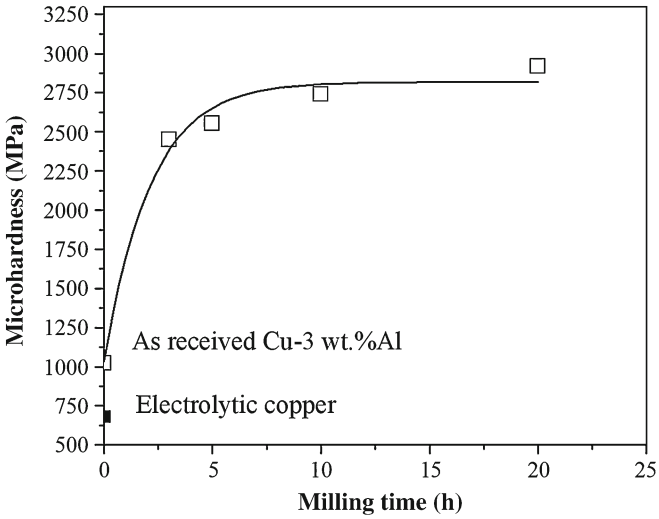

Figure 5. Effect of milling time on microhardness of Cu–3 wt.%Al compacts.

in copper matrix by internal oxidation of prealloyed copper with 3 wt.% aluminium.

X-ray diffraction pattern of Cu–3 wt.%Al powder shows a progress in line broadening with milling time (figure 3), as a result of a severe lattice distortion and crystallite size refinement (Ziegler 1978; Lonnberg 1994).

The effect of milling time on the crystallite size and lattice distortion of examined powder particles is presented in figure 4. As can be seen, the most intensive crystallite refinement occurs in the early stage of milling when the crystallite size abruptly decreases from about 542 to about 55 nm, whereas in the period from 5 h to 20 h the crystallite size remains practically constant, i.e. approximately 30 nm. Figure 4 also illustrates a strong increase of lattice distortion during 5 h of milling. At longer milling time the lattice distortion becomes less evident. This result is in agreement with some earlier hypothesis that the deformation of particles occurs during the early stage of milling (Ziegler 1978).

Microhardness of compacts depends on the previous milling time of prealloyed copper powder (figure 5). Microhardness of all compacts increases with the milling time showing that 20 h milled compacts exhibit significantly higher microhardness (up to 2940 MPa) than compacts processed from as-received powders (1020 MPa). The change in microhardness occurs within 5 h of milling and prolonged milling results in a negligible change in microhardness. Since after 5 h of milling (see figure 4), the crystallite size is completely decreased which suggests that small crystallite size has a very strong effect on hardening of Cu–3 wt.%Al. In spite of the fact that the data on alumina particles formed during internal oxidation were not known, the effect of these particles on microhardness cannot be neglected. The microhardness (2550 MPa) of compact processed from 5 h-milled powder with crystallite size of about 55 nm is 3·5 times greater than that processed from as-received electrolytic copper powder (667 MPa) compacted under the same conditions. The coarsening of alumina particles leads to lowering of microhardness, but since in the case of this study

Table 1. Effect of high temperature exposure at 800°C for 5 h on crystallite size and microhardness of Cu–3 wt.% Al compacts processed from 5 and 20 h milled powders.

	Before exposure Milling time (h)		After exposure Milling time (h)	
	5	20	5	20
Crystallite size (nm)	75	45	82	49
Microhardness (MPa)	2550	2940	1790	2790

microhardness remains constant up to 20 h of milling, it may be assumed that the coarsening of alumina dispersoids did not occur, or the effect of small crystallite size dominates over the process of hardening. This assumption confirms the results published by Mehta *et al* (1990) and Nadkarni and Synk (1984), which reported that alumina content above 0·65wt.% did not result in increase of hardening.

The results of the effect of high temperature exposure at 800°C for 5 h on the crystallite size and microhardness of compacts processed from 5 and 20 h-milled powders are shown in table 1. In general, Cu–3 wt.%Al compacts are characterized by low increase in the crystallite size and by low decrease in the microhardness as a consequence of the presence of very fine Al_2O_3 particles. A previous investigation (Rajkovic and Mitkov 2000) showed that most of alumina particles formed *in situ* by oxygen from the air are finer than 100 nm and well within the range required for the dispersion hardening (Benjamin 1970).

As far as properties of compacts are concerned, the measured density of compacted Cu–3 wt.%Al powder after 5 h and 20 h of milling (7·74 and 7·85, respectively) in comparison with theoretical (8·46 gcm^{-3}) were 93·1% and 94·5% indicating that the densification by hot pressing of milled prealloyed powder was not completed. Hot extrusion seems to be a common method of compaction because the measured density of Cu-based extruded composites is greater than 99·3% (Preston and Grant 1961).

Figure 6 illustrates the microstructure of as-received and milled Cu–3 wt.% Al powder particles (figures 6(a) and (c), respectively) and composites after 0 h and 20 h of milling (figures 6(b) and (d), respectively). Comparing the microstructure of the as-received powder (figure 6(a)) with the milled powder particles (figure 6(c)), it is evident that milled powder particles exhibit lamellar structure typical for high energy treated powders, where lamellae represent individual plastically deformed prealloyed copper particles. Figure 6(d) shows that the lamellar structure of particles is retained in composite, i.e. following hot-pressing. The light areas (denoted by arrows) in the microstructure of Cu–3 wt.% Al composite (figure 6(d)) indicate that recrystallization occurred during hot-pressing. The recrystallization in Cu–3 wt.% Al composite was initiated at the corners of the

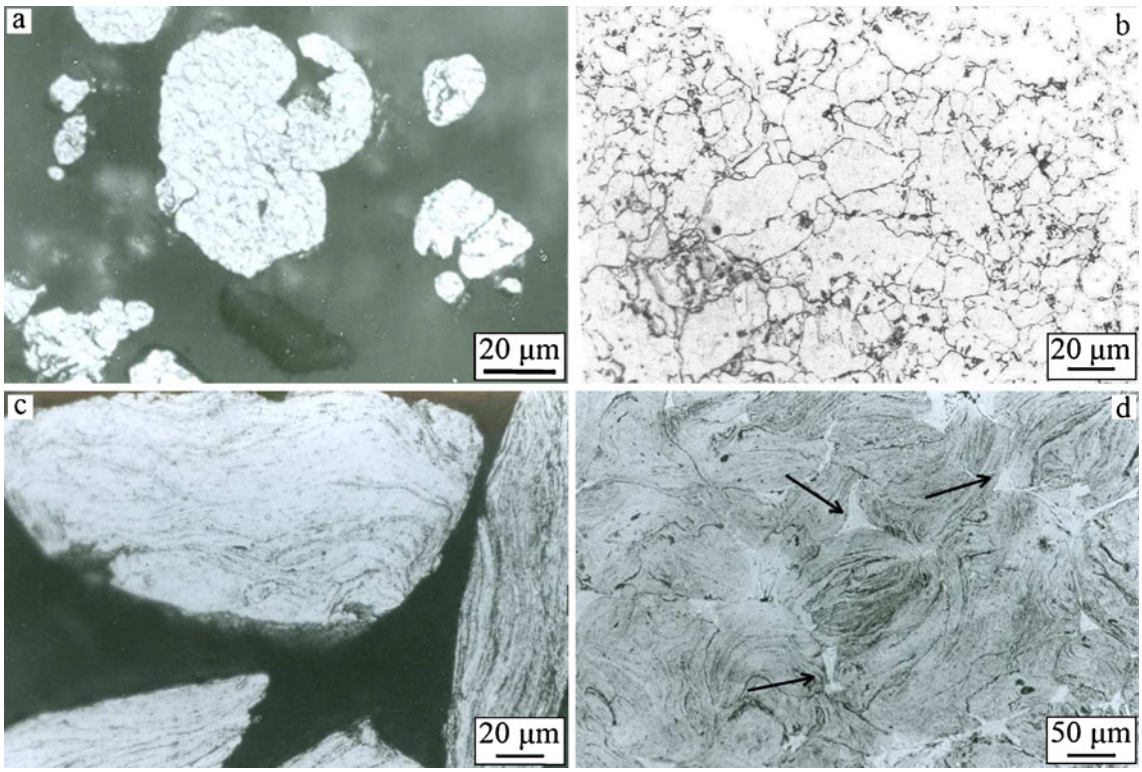

Figure 6. OM micrographs showing microstructures of Cu–3 wt.% Al powders and compacts: **a.** as-received powder; **b.** as-received hot compacted powder; **c.** 20 h-milled powder and **d.** hot compacted 20 h-milled powder.

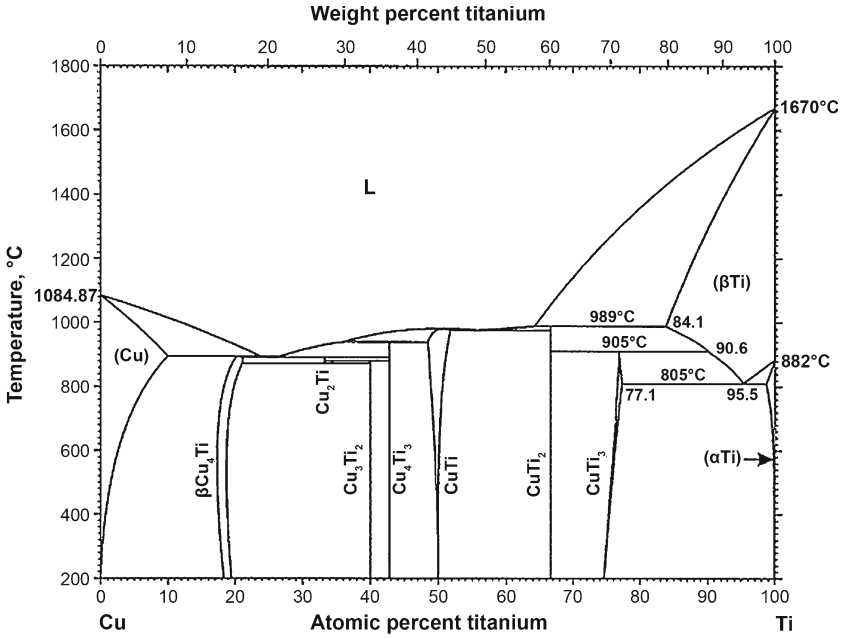

Figure 7. Cu–Ti phase diagram.

particle powder where the concentration of stresses imposed during compaction was the highest.

3.2 *Cu–0·6 wt.%Ti–2·5wt.%TiB_2 alloy*

The eutectic of the binary Cu–Ti and Cu–B alloys is about 1000°C (Chakrabarti and Laughlin 1982; Massalski *et al* 1986) (figures 7 and 8), and this temperature was the basic parameter for the preparation of master alloys (table 2).

As-cast homogeneous microstructure dendrite morphology of master alloys is illustrated in figure 9. Using a copper casting mould, improved homogenization was obtained, resulting in randomly distributed alloying elements in a copper matrix. A dendritic morphology predominates in the microstructure (figures 9(a) and (b)). A large quantity of equilibrium β phase may be observed in the prealloyed structure (figure 9(a), arrows), and this is due to the relatively low solidification rate.

Using the as-cast master alloys the composite powder particles were produced by gas atomization according to the previously described procedure. The nominal chemical composition of powders obtained by gas atomization is Cu–0·6Ti–2·5TiB_2 (wt.%) (in the further text this material will be referred to as Cu–Ti–TiB_2). The diameter of particles, d, was in the range $50 < d < 500$ μm. The sieving method was applied with the purpose to obtain the range of particle sizes. After completing the gas atomization, microstructural characterization of the obtained powder was undertaken. The quantitative investigation of atomized Cu–Ti–TiB_2 powder particles obtained by chemical analysis and their microhardness as a function of their size are given in table 3.

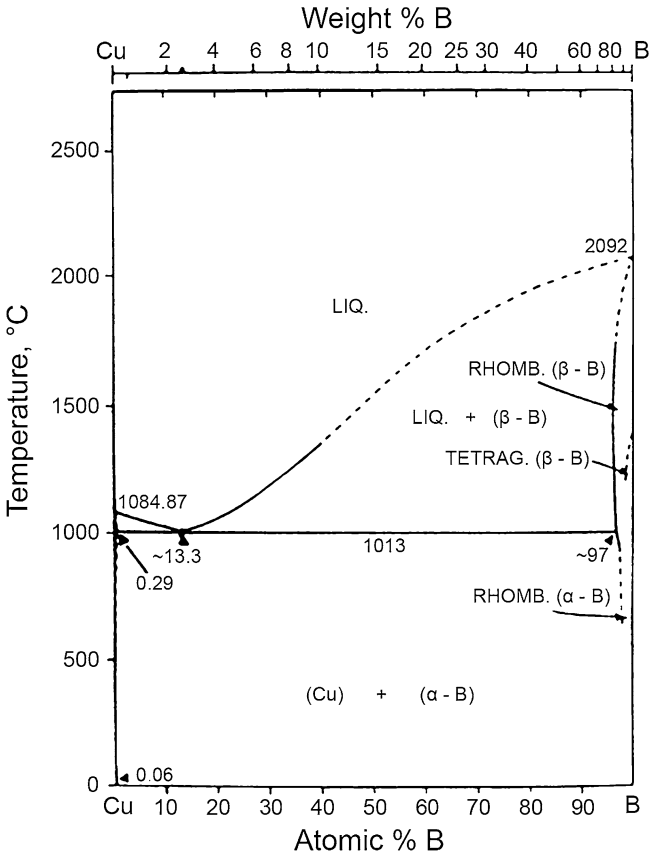

Figure 8. Cu–B phase diagram.

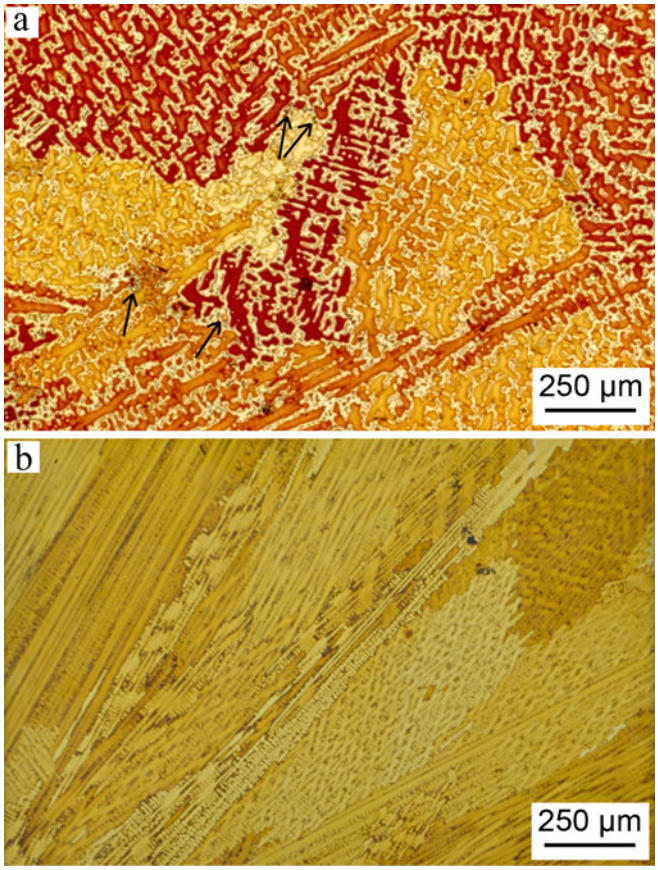

Figure 9. OM micrographs showing microstructure of as cast: **a.** Cu–3·8Ti (wt.%) and **b.** Cu–1·2B (wt.%) master alloys.

The alloy particles are spherical in shape with homogenous structure and characteristic dendrite morphology. The homogenous distribution of TiB_2 particles in the microstructure could not be observed using optical microscopy (figure 10), but its presence reflects the microhardness values. Comparing the results of tables 2 and 3 it is evident that the microhardness of gas atomized particles is higher than microhardness of as-cast master alloys. Analysis of microstructure and determination of microhardness did not include small particles (satellites) in figure 10(c). Although structural parameters (grain size, solid solution) affect hardness, our earlier researches (Bozic and Mitkov 1992) show that the homogenous distribution of TiB_2 particles was the dominant factor.

The XRD analysis of atomized powders showed only the presence of TiB_2 phase in the copper matrix (figure 11). However, using an additional chemical analysis (see table 3) the presence of certain amounts of titanium and a negligible amount of boron was identified.

Diffusivities of titanium and boron in copper were calculated (figure 12) using the diffusion coefficient values for titanium and boron in copper at 800°C and 900°C already reported in the literature, and an extrapolation of the literature data. It was shown that the convergence of the obtained results with the increase in temperature is the result of a lattice expansion (Rexer 1972). The increase in the diffusion coefficients with increasing temperature points out that small independent concentrations of titanium and boron require longer times for the formation of TiB_2 at lower temperatures, whereas the formation of dispersoids is very rapid *in situ* during the atomization process (1400°C).

An increase of microhardness in the as-atomized powders should be explained by homogeneous distribution of very hard TiB_2 particles in the primary matrix (table 3). The

Table 2. Basic characteristics of as cast master alloys used for Cu–Ti–B alloys production.

Composition of master alloy (wt.%)	Casting temperature (°C)	Holding duration at casting temperature (min)	Composition of as-cast material (wt. %)	Hardness (MPa)
Cu–4Ti	1100	10	Cu–3·8Ti	1863
Cu–1·4B	1100	10	Cu–1·2B	1147

Table 3. Characteristics of Cu–Ti–B atomized powders.

Composition of as-cast master alloy (wt.%)	Chemical analysis of as atomized material (wt.%)		Microhardness (MPa)		
	Ti	TiB_2	$d^* < 80$ μm	80 μm $< d^* <$ 150 μm	200 μm $< d^* <$ 500 μm
Cu–3·8Ti + Cu–1·2B	0·6	2·5	2256	2260	2246

*Powder particles size.

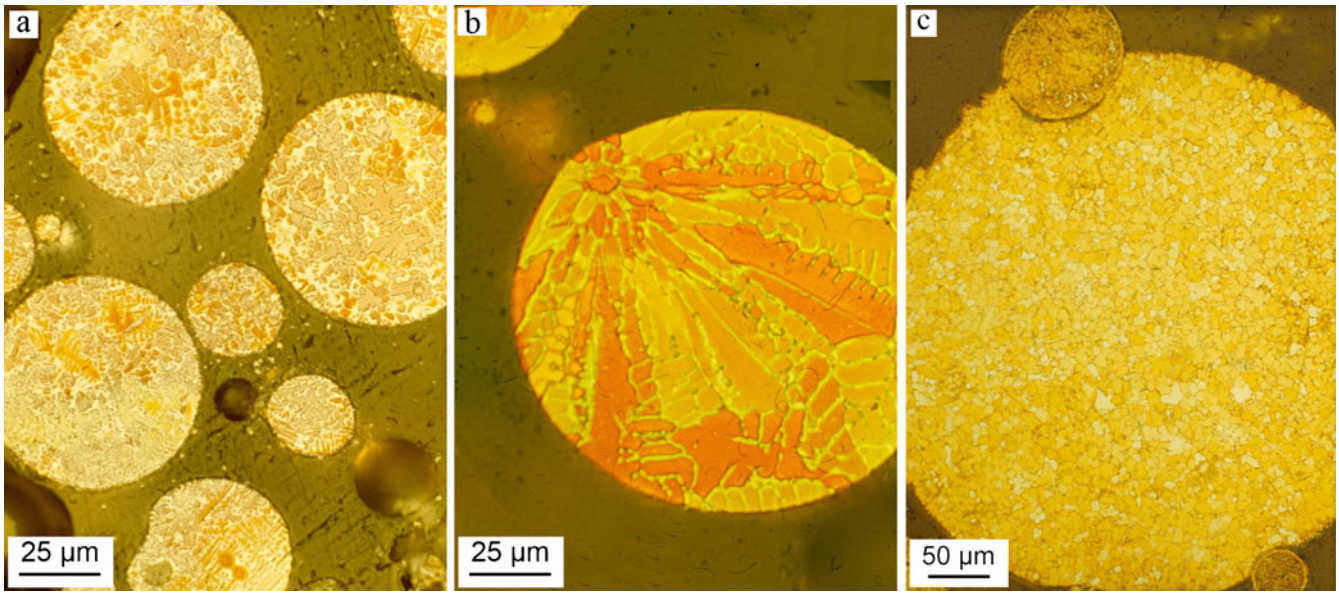

Figure 10. OM micrographs showing microstructure of different as-atomized Cu–0·6Ti–2·5TiB_2 (wt.%) alloy powder sieving fractions: **a.** $d < 80$ μm, **b.** 80 μm $< d <$ 150 μm, and **c.** 200 μm $< d <$500 μm.

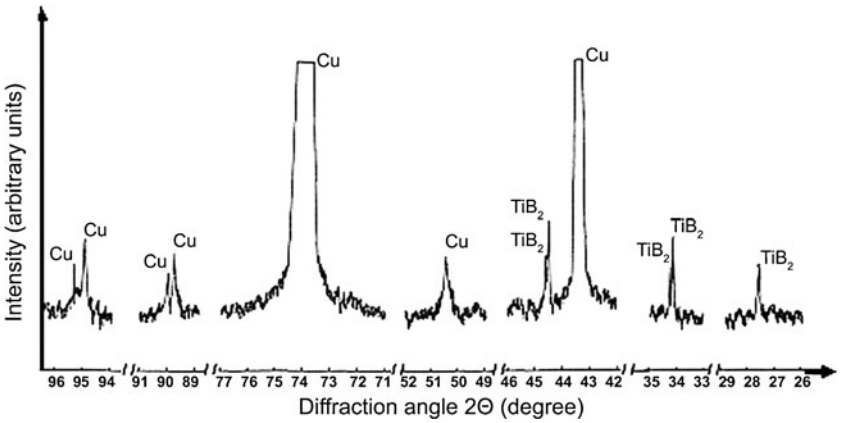

Figure 11. XRD pattern of Cu–TiB_2 powder.

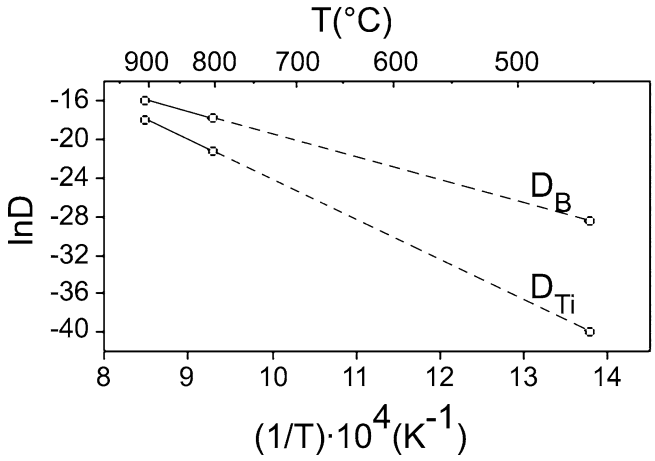

Figure 12. Calculated diffusion coefficients for titanium and boron in copper.

microhardness presented in table 3 reveals the surprising fact that the decrease in powder particle size does not affect the microhardness values. Detailed research of this phenomenon is given in another paper (Bozic and Mitkov 1994) showcasing several alloys of different composition of alloying materials from Cu–Ti–B system. From the present results it may be assumed that the distribution of the dispersoids in the powder structure has a much greater influence on the powder particle microhardness than the particle size itself.

It is well known that compaction of spherical particles of different sizes results in lower compacts porosity. That is, during the compacting treatment smaller powder particles will fill in the empty spaces between larger neighbouring spherical particles. In this way the powder apparent density can reach even 60% of the theoretical material density facilitating easier powder compaction (German 1994).

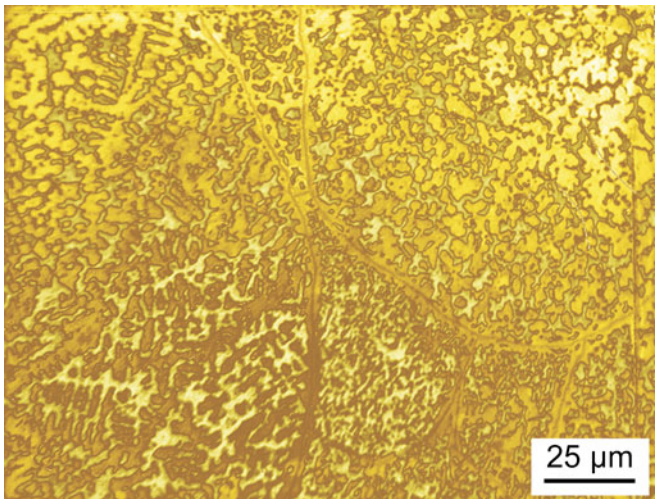

Figure 13. OM micrograph showing microstructure of HIP-ed Cu–Ti–TiB_2.

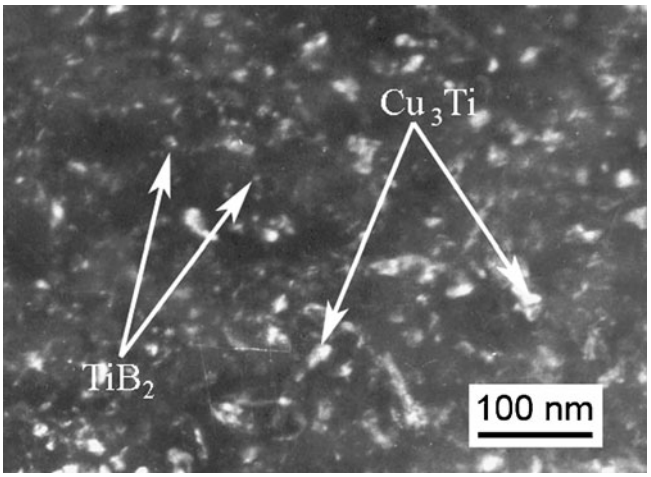

Figure 14. TEM micrograph showing dispersoid TiB_2 particles and Cu_3Ti equilibrium precipitates present in copper matrix.

For compaction, the powder mixture consisting of spherical particles of different sizes was used without any concern that this can bring about the variation in the compact microhardness (results presented in table 3 clearly show that the microhardness values are practically identical for different powder fractions). An investigation of Cu–Ti–TiB_2 composites produced by gas atomization and HIP-ing was challenging because of the insufficient literature data available. The main concern was compacting composites with fine and hard dispersoid particles to near theoretical density without changing the rapidly solidified microstructure. Nearly non-porous compacts of Cu–Ti–TiB_2 composite were produced by HIP-ing and rapid quenching to room temperature (figure 13 and table 4).

During HIP, the densification occurs as a result of powder particles deformation near the surface of their contacts, power law creep and diffusion. The overall behaviour of materials under the influence of applied pressure and high temperature is very complex because all of the above-mentioned densification mechanisms depend on the particle size, processing parameters and other material properties in a different way. From figure 13 and the data presented in table 4, one can conclude that parameters selected for the HIP-ing process provided sufficient atomic mobility, which is necessary for the high pressure sintering completion and elimination of porosity. At 750°C the material deformation induced by thermally activated dislocation movements is possible, and therefore, time-dependent densification mechanisms (above all, power law creep and diffusion) were significant in relation to the overall densification rate. It can also be noticed (figure 13 and table 4) that the microstructure degradation and microhardness change of the produced composite compacts did not occur.

Contrary to the rapidly solidified powders where only the presence of TiB_2 dispersoids was identified, in the TEM micrograph of HIP-ed compacts coarse particles of Cu_3Ti precipitates can also be distinguished (figures 14 and 15). This microstructure is a consequence of lower cooling rates after sintering, compared to cooling rates after atomization. The presence of equilibrium Cu_3Ti precipitates causes a decrease of microhardness values in relation to powders (see tables 3 and 4). A uniform distribution of *in situ* formed TiB_2 dispersoids in the metal matrix may also be observed in figures 14 and 15. This distribution of the dispersoids which was achieved during the atomization processing was retained during HIP-ing.

The behaviour of HIP-ed composite compacts after solution treatment and aging is typical for alloys strengthened by spinodal decomposition (Cahn 1963; Kato *et al* 1980; Ardell 1985). The maximum hardness values apparent after aging at 350°C for 5 min (the hardening effect in the early stage, figure 16) is most likely due to the presence of a modulated structure. The spinodal decomposition involves the continuous transformation of a disordered to an ordered $Cu_4Ti_{(m)}$ phase, which is in equilibrium with the *fcc* copper solid solution. The hardening effect in the early stage is due to the effect of internal stresses, the self-energy gradient, and

Table 4. HIP-ing parameters and properties of obtained Cu–Ti–TiB_2 composite.

Composition of as HIP-ed materials (wt.%)	Temperature (°C)	Time (min)	Pressure (MPa)	Density (g/cm^{-3})	Open porosity (%)	Microhardness (MPa)
Cu–0·6Ti–2·5 TiB_2	750	10	200	8·43	0·05	2059

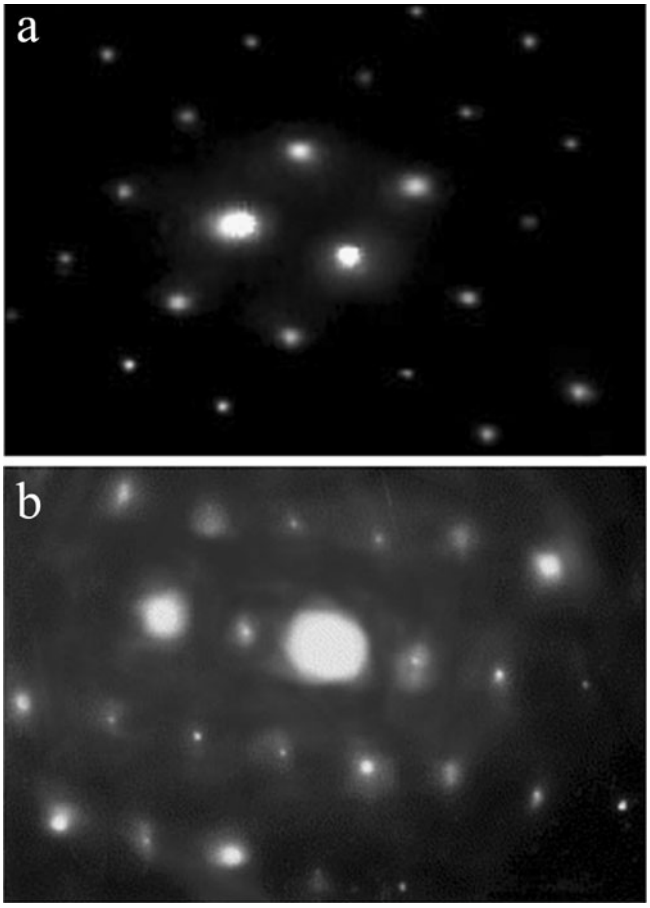

Figure 15. SAD pattern of TiB_2 **a.** and Cu_3Ti **b.** particles in copper matrix.

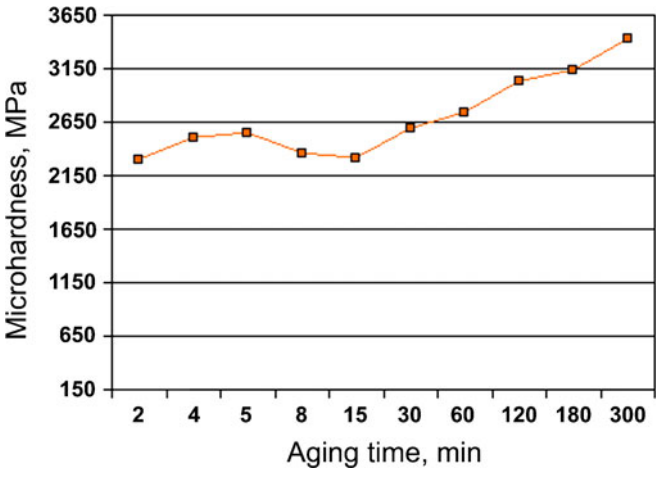

Figure 16. Hardness of HIP-ed Cu–Ti–TiB_2 composite aged at 350°C vs time of aging.

chemical hardening. According to Cahn (1963), Kato *et al* (1980) and Ardell (1985), the motion of combined dislocations in the periodic deformation field is strongly dependent on the statistical configuration of obstacles present in the

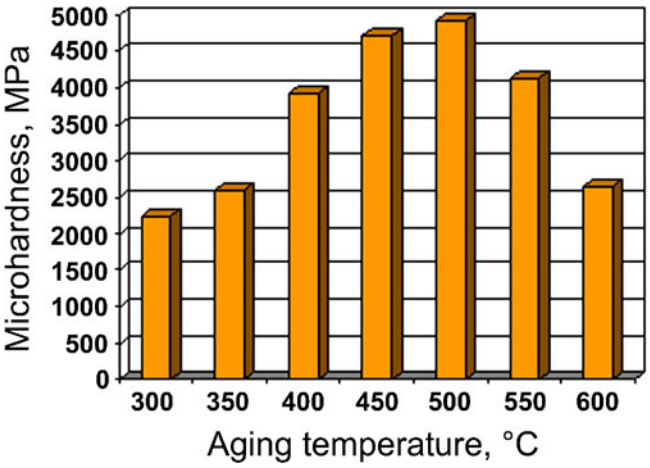

Figure 17. Hardness of HIP-ed Cu–Ti–TiB_2 composite vs aging temperature, for 30 min.

system. The structural ordering in the titanium rich regions causes the disappearance of antiphase boundaries resulting from lattice misfit. Easier dislocation motion through such an ordered structure leads to a hardness decrease (figure 16, aging between 5 and 15 min). With prolonged time of aging the hardening effect is due to the intensified coherent precipitation of $Cu_4Ti_{(m)}$ particles extending antiphase boundary formation (Kratochvil *et al* 1980).

Compared to a binary Cu–Ti alloy with similar titanium content (0·58 wt.% Ti) (Bozic and Mitkov 1991), the Cu–Ti–TiB_2 composite yields much higher microhardness values, owing to primary TiB_2 dispersions formed *in situ,* during atomization. Except for increased starting microhardness value (which remains nearly unchanged at high annealing temperatures) and strengthening intensity after aging, the presence of finely distributed TiB_2 dispersoids shows a positive effect on the mechanical stability of matrix on higher precipitation temperatures (figure 17).

4. Conclusions

The following conclusions can be drawn from the present study:

(I) The decrease of Cu–3 wt.%Al lattice parameter with milling time was the result of oxidation of aluminum which precipitated from prealloyed copper forming a fine dispersion of Al_2O_3 particles. Assuming that the complete amount of aluminum was oxidized, it was calculated that 5·6 wt.% of Al_2O_3 was produced in the copper matrix by internal oxidation of 3 wt.% Al.

(II) Increase in microhardness of Cu–3 wt.%Al composites is a consequence of very small crystallite size formed during high energy milling of starting and the

presence of very fine alumina particles generated by internal oxidation. The microhardness of compacts processed from the as-received Cu–3 wt.%Al powder was 1020 MPa, whereas in the case of composites originating from milled powders microhardness increased up to 2940 MPa.

(III) During high-temperature exposure at 800°C Cu–3 wt.%Al composites retain relatively high microhardness which indicates their high thermal stability.

(IV) The milled Cu–3 wt.%Al powder particles exhibit lamellar structure typical for high energy treated powders where lamellae represent individual plastically deformed prealloyed copper particles. The lamellar structure of particles is retained in composites, i.e. following hot-pressing.

(V) The homogeneous distribution of alloying elements in the Cu–Ti–B prealloy during atomization is highly dependent on the correct choice of titanium and boron amounts, as well as on appropriate melting parameters.

(VI) Successful preparation of the *in situ* formed TiB_2 dispersoids in copper matrix powders was achieved via argon atomization at 1400°C.

(VII) Rapidly solidified Cu–Ti–TiB_2 powders are characterized by the presence of finely dispersed TiB_2 particles for which the main reason is for the high microhardness values of Cu–Ti–TiB_2 powders.

(VIII) Nonporous compacts of Cu–Ti–TiB_2 composite with homogenous microstructure and high microhardness values were obtained during 10 min of HIP-ing at 750°C under applied argon pressure of 200 MPa. Starting microstructure morphology of the rapidly solidified powder particles was not disturbed after HIP-ing, whereas a uniform distribution of the TiB_2 particles in the copper matrix was attained.

(IX) High strengthening of Cu–Ti–TiB_2 compacts is achieved by thermal treatment (aging) as a consequence of the simultaneous influence of the following factors: the development of modular structure, the precipitation of metastable $Cu_4Ti_{(m)}$, and the presence of TiB_2 dispersoid nanoparticles.

Acknowledgement

The results presented are realized with financial support of Ministry of Science and Technological Development of the Republic of Serbia through project No. 172005.

References

Ardell A J 1985 *Metall. Trans. A, Phys. Metall. Mater. Sci*. **16** 2131
Benjamin S J 1970 *Metall. Trans*. **1** 2943
Bozic D and Mitkov M 1991 *Powder Metall*. **34** 199
Bozic D and Mitkov M 1992 *Mater. Sci. Technol*. **8** 1108
Bozic D and Mitkov M 1994 *J. Mater. Sci. Lett*. **14** 204
Cahn J W 1963 *Acta Metall*. **11** 1275
Chakrabarti D J and Laughlin D E 1982 *Bull. Alloy Phase Diag*. **3** 45
German R M 1994 *Powder metallurgy science* (Princeton, NY, USA: MPIF) 2nd ed., p. 142
Kato M, Mori T and Schwartz L H 1980 *Acta Metall*. **28** 285
Kratochvil P, Saxlova M and Pesicka J 1980 *5th International conference on strength of metals and alloys proceedings* (eds) P Haasen *et al* (New York, USA: Pergamon) **2** p. 687
Kuruvilla A K, Prasad K S, Bhanuprasad V V and Mahajan Y R 1990 *Scr. Metall. Mater*. **24** 873
Lawley A and Apelian D 1994 *Powder Metall*. **37** 123
Lee J S, Jung J Y, Lee E S, Park W J, Ahn S and Nack J K 2000 *Mater. Sci. Eng.* **A277** 274
Lonnberg B 1994 *J. Mater. Sci*. **29** 3224
Ma Z Y, Tjong S C and Wang Z G 1999 *Mater. Sci. Eng.* **A264** 177
Ma Z Y, Tjong S C and Gen L 2000 *Scr. Mater*. **42** 367
Massalski T B, Murrey J L, Bennett L H and Baker H (eds) 1986 *Binary alloy phase diagrams* (Metals Park, Ohio: ASM)
Mehta M L, Ghudbban T K A, Elthalhi M S B and Elraby N E A 1990 *Powder Metall. Int*. **22** 15
Nadkarni V N and Synk E J 1984 *Metals handbook* (Metals Park, Ohio: Powder Metallurgy ASM) p. 711
Naser J, Riehemann W and Ferkel H 1997 *Mater. Sci. Eng.* **A234–236** 467
Preston O and Grant J N 1961 *Trans. Metall. Soc. AIME* **221** 164
Rajkovic M V and Mitkov V M 2000 *Int. J. Powder Metall*. **36** 45
Rajkovic V, Bozic D and Jovanovic T M 2006 *Kovove Mat*. **44** 175
Ralph B, Jyen H C and Lee B 1997 *J. Mater. Process. Technol*. **63** 339
Rexer J 1972 *Z. Metallkd*. **63** 745
Tjong S C and Lau K C 2000 *Mater. Sci. Eng.* **A282** 183
Tjong S C, Ma Z Y and Li R K Y 1999 *Mater. Lett*. **38** 39
Tu J P, Wang N Y, Yang Y Z, Qi W X, Liu F, Zhang X B, Lu H M and Liu M S 2002 *Mater. Lett*. **52** 448
Williams G K and Hall W H 1953 *Acta Metall*. **1** 22
www.semitracks.com/index.php/en/reference-material/material-properties
Ziegler G 1978 *Powder Metall. Int*. **10** 70